Available online at www.sciencedirect.com
SCIENCE DIRECT®
Earth and Planetary Science Letters 222 (2004) 161–175
EPSL
www.elsevier.com/locate/epsl

Towards a lower mantle reference temperature and composition

Frédéric Deschamps*, Jeannot Trampert

Department of Geophysics, Utrecht University, Budapestlaan 4, P.O. Box 80021, 3508 TA Utrecht, The Netherlands

Received 15 July 2003; received in revised form 16 February 2004; accepted 16 February 2004

Abstract

We aim to constrain the lower mantle geotherm and average composition from 1D seismic models and experimental mineralogy data, explicitly accounting for possible sources of uncertainty. We employ an isentropic third-order Birch–Murnaghan equation of state, which is in excellent agreement with recent ab initio calculations of density and bulk modulus for Mg-perovskite. Furthermore, ab initio and experimental data are reasonably consistent with each other. Modelling the shear modulus is not as straightforward, but is needed because density and the bulk modulus alone do not sufficiently constrain temperature and composition. To correctly predict ab initio calculations for the shear modulus of Mg-perovskite, we needed to prescribe a cross-derivative at zero pressure, which we determined by trial and errors. Unless this ad hoc cross-derivative is confirmed by further experimental results, there seems to be an inconsistency between ab initio and experimental data. Purely experimental data most likely require a non-adiabatic temperature profile, but it is difficult to infer the number and location(s) of the non-adiabatic increase(s). If ab initio data are used, at least one thermal boundary layer seems reasonable, but its location depends on the modelling of the iron content. A strong chemical density contrast in the mid-mantle ($\geq 2\%$) is not supported by ab initio data, but is possible with experimental data. Other major sources of uncertainty are the trade-off between thermal and compositional effects, the possible influence of aluminium perovskite, and poorly understood frequency effects.

Keywords: Mg-perovskite; thermal boundary layer; aluminium perovskite

1. Introduction

The Earth's average profiles of temperature and composition are key parameters to understand mantle dynamics, but to date, they are only poorly known. Anchoring points at the bottom of the upper mantle [1,2] and at the core–mantle boundary (CMB) [3,4] give a rough idea of the temperature increase through the lower mantle. A typical value for the non-adiabatic contribution is $\Delta T = 1000$ K, but the error is large, about ± 500 K. Anderson [4] used these anchoring points and different average properties of the lower mantle to compute an average temperature profile. The most detailed information about the average Earth's structure comes from radially symmetric seismic models, such as PREM [5]. These 1D-models provide a good description of the elastic moduli of the mantle, but inferring average temperature and composition from them is not straightforward. Brown and Shankland [6] computed entropies from seismic models, and deduced the mantle temperature. Alternatively, working along an adiabat

* Corresponding author. Tel.: +31-30-253-5135.
E-mail address: deschamp@geo.uu.nl (F. Deschamps).

0012-821X/$ - see front matter © 2004 Elsevier B.V. All rights reserved.
doi:10.1016/j.epsl.2004.02.024

(e.g., [7,8]) one can choose a potential temperature that fits the seismic models, and compute a temperature profile from the adiabatic gradient. For the lower mantle, Shankland and Brown [9] found an adiabatic contribution of 600 K. Average composition can also be tested against seismic models. Jeanloz and Knittle [10] used the density of PREM to estimate the temperature and the volumetric fraction of iron in the lower mantle. To date, there is still no consensus on the average temperature and composition, as illustrated by recent studies [11–13] that propose very different results.

Inferring the mantle temperature and composition from seismic models requires a careful equation of state (EOS) modelling and accurate knowledge of the thermoelastic properties of minerals [11]. Modelling the shear modulus is particularly difficult because still few data are available. Jackson [11] showed that third-order Eulerian finite strain isotherms and isentropes appear adequate for the range of strains encountered in the lower mantle. Furthermore, he showed that working along hot finite strain isentropes is consistent with the Mie–Grüneisen–Debye description of thermal pressure. Stacey [14] observed that the shear modulus varies linearly with pressure and the bulk modulus along adiabats, which is compatible with a Birch–Murnaghan adiabatic compression to third-order [11,15]. Ideally, we should move away from EOS modelling and use directly high-temperature and high-pressure data. Recent progress in ab initio calculations started to give us this possibility, but data are still scarce. da Silva et al. [12] inferred temperature from ab initio data of the bulk modulus of Mg-perovskite alone, but this resulted in large uncertainties, even for a fixed average composition. Marton and Cohen [13] used ab initio calculations for the shear modulus at high temperature and pressure, and they find a small value of the volumetric fraction of perovskite. In addition to these difficulties, seismic models cannot fully resolve the average mantle temperature and composition and as a result, trade-offs between temperature and other parameters allow a large range of temperatures and compositions to fit 1D seismic models [11,16,17].

There is mounting evidence that thermo-chemical convection is likely to occur in the mantle, but the mode of convection is still a matter of debate, in particular the location(s) and thickness of thermal boundary layer(s) and of chemical layer(s). A good candidate is the D″ layer, which culminates 200–300 km above the CMB, where oceanic crust transformed into eclogite could sediment [18,19]. In that case, D″ remains stable if the chemical density contrast ($d\rho_c$) is higher than 2% [18,20]. Alternative models proposed a more complex structure [21,22]. Davaille [21] showed that for appropriate chemical density contrasts, oscillatory domes are able to develop in a stratified fluid. Kellogg et al. [22] explained several geophysical observations with a model of descending slabs deflecting a dense lower layer.

In the present paper, we test a collection of models against density and the elastic moduli of PREM. We make no assumption on temperature or composition and determine what can actually be constrained by 1D seismic models. Our EOS modelling is partly designed to fit all recently available ab initio data. This makes results largely modelling-independent, and allows to reasonably fill existing gaps in current ab initio data. These results are compared to the classical use of third-order Birch–Murnaghan equation of state with available experimental data. We also focus on the influence of corrections for the volumetric fraction of iron in elastic moduli, which are important in some cases.

2. Method and data

We reconstruct density and seismic velocities of the lower mantle from thermoelastic properties of minerals and appropriate equations describing these properties as a function of temperature and pressure, following [15]. The density (ρ) and the adiabatic bulk modulus (K_S) of each mineral composing the rock are heated (at zero pressure) to the potential temperature T_p using:

$$\rho(T_p, P=0) = \rho_0 \exp\left[-\int_{T_0}^{T_p} \alpha(T)\mathrm{d}T\right] \quad (1)$$

$$K_S(T_p, P=0) = K_{S0} \exp\left[\frac{\rho(T_p, P=0)}{\rho_0}\right]^{\delta_{S_0}} \quad (2)$$

where α is the thermal expansion, $\delta_S = -1/(\alpha K_S)\dot{K}_{S0}$ is the Anderson–Grüneisen parameter, and $\dot{K}_{S0}$ is the

temperature derivative of K_S at constant pressure. The subscript '0' stands for ambient temperature and pressure. For the shear modulus (G), we used a linear projection:

$$G(T_p, P=0) = G_0 + \dot{G}_0(T_p - T_0) \quad (3)$$

where $\dot{G}_0$ is the temperature derivative of G at constant pressure. The justification for Eqs. (2) and (3) is given in [15] on the basis of MgO data. To extrapolate ρ, K_S and G at pressure P, we use a Birch–Murnaghan adiabatic compression to the third-order in strain (BM3). The pressure is then given by:

$$P = -3K_{S0}(1-2\varepsilon)^{5/2}\left[\varepsilon + \frac{3}{2}(4 - K'_{S0})\varepsilon^2\right] \quad (4)$$

where K'_{S0} is the pressure derivative of the bulk modulus at constant entropy, and ε the Eulerian strain. The pressure is known relatively well from PREM, which determines ε. This allows to calculate the density from:

$$\rho(T,P) = \rho(T,P=0)(1-2\varepsilon)^{3/2} \quad (5)$$

and the bulk modulus to third-order using:

$$K_S = K_{S0}(1-2\varepsilon)^{5/2} \times \left[1 + (5 - 3K'_{S0})\varepsilon - \frac{27}{2}(4 - K'_{S0})\varepsilon^2\right] \quad (6)$$

A similar equation defines the shear modulus (G) (e.g., [7]). Alternatively, Stacey [14] proposed a linear relation valid along an adiabat:

$$G = A\,K_S - BP \quad (7)$$

where the constants A and B are determined at $P=0$ and T_p. We checked that these two extrapolation methods for G lead to the same results. The density and the elastic moduli of the mineralogical assemblage are finally deduced from volumetric and Voigt–Reuss–Hill averages, respectively. Densities and elastic moduli of minerals also depend on the volumetric fraction of iron (X_{Fe}). When data are available (Table 1), we account for this dependency at $P=0$ and $T_p=298$ K. It is convenient to use the global volumetric fraction of iron in the aggregate Fe_{glob}. The values of X_{Fe} for perovskite and magnesio-wüstite are then deduced from Fe_{glob} and from the iron partitioning K_{Fe} between perovskite and magnesio-wüstite. Calcium perovskite may also enter the composition of the lower mantle and influence the density and elastic moduli of the mantle aggregate. We account for this dependence in a similar way as we do for the iron dependence, using recent experimental measurements and ab initio calculations [29,30]. Compression induces an increase of temperature, and to get the mantle (or final) temperature one must add an adiabatic contribution to the potential temperature. We calculated this increase from the adiabatic temperature gradient:

$$\left(\frac{\partial T}{\partial P}\right)_S = \frac{\gamma T}{K_S} \quad (8)$$

In the quasi-harmonic approximation, the Grüneisen parameter γ is given by:

$$\gamma = \gamma_0\left(\frac{\rho}{\rho_0}\right)^q \quad (9)$$

where q is a constant. Taking q from Table 1, and knowing ρ from Eq. (5), we can evaluate γ and thus T. The values of the thermoelastic parameters used in the present paper are listed in Table 1. When available, we indicate either the error bars on the measurements, or a range of possible values based on data published in different studies.

Error bars on the thermoelastic parameters result in uncertainties on the extrapolated elastic moduli. Other sources of uncertainty are the assumed potential temperature and the exact composition of the aggregate. When all those parameters are varied within reasonable ranges (defined below), one obtains a collection of profiles for density, the elastic moduli, and the seismic velocities. On average, we find variations of about 0.05 g/cm^3 on density and 20 GPa on the elastic moduli. Some of these models are not suitable to describe the Earth's mantle, and realistic models must fit density and elastic moduli of PREM within a given range. The choice of PREM as a reference model might influence the results. We repeated most of the calculations with the reference model ak135 [31], but did not find any significant differences. A statistical analysis of the selected models provides an estimate of the average mantle

Table 1
Thermoelastic properties of $MgSiO_3$ and MgO[a]

	Perovskite			Magnesio-wüstite	
	Experimental	Ab initio[b]	C_{Fe}[c]		C_{Fe}[c]
ρ (g/cm^3)	4.109	4.107	+1.03[d]	3.584	2.28
K_{S0} (GPa)	264.0	268.9	+20[d]	162.5	11.5[e] /+18.0[f]
K'_{S0}	3.97/3.95/3.77/3.75[e]	4.07	+0.16[d]	4.0[g] to 4.15[h]	−0.53[f]
$\dot{K}_{S0}$ (10^{-2} GPa/K)	−1.1/−1.5/−1.0/−1.5[e]	−1.2	–	−1.55[i] to 1.4[h]	–
G_0 (Gpa)	175.0	180.0	−40[g]	130.8	−75.6[e]/−108[f]
G'_0	1.8 (0.4)	–	−0.52[d]	2.4[g] to 2.5	−3.29[f]
$\dot{G}_0$ (10^{-2} GPa/K)	−2.9 (0.3)	–	–	−2.4 to −2.2[h]	–
γ_0	1.31/1.39/1.33/1.41[e]	1.51	–	1.41	–
q	1.0/2.0/1.0/2.0[e]	1.27	–	1.3	–
a_1 (10^{-5} K^{-1})	1.19 (0.17)	2.066	–	3.681	–
a_2 (10^{-8} K^{-2})	1.20 (0.10)	0.909	–	0.9283	–
a_3 (K)	0.0	0.418	–	0.7445	–

[a] All data are from the compilation of Trampert et al. [15] unless otherwise stated. When available, error bars are indicated in parenthesis. ρ is the density, K_{S0} the adiabatic bulk modulus, G_0 the shear modulus, γ_0 the Grüneisen parameter at ambient temperature and pressure, and q a constant. Primes and dots denote derivation with respect to pressure and temperature, respectively. Thermal expansion at P=0 is calculated following $\alpha=a_1+a_2T-a_3T^{-2}$.

[b] Properties of $MgSiO_3$ deduced from the ab initio calculations of Oganov et al. [23].

[c] Correction for the iron content. Given the volumetric fraction of iron X_{Fe}, the corrected value for a parameter M is $M_{Mg,Fe}=M_{Mg}+C_{Fe}X_{Fe}$.

[d] [24].

[e] Jackson [11]. Four alternative combinations of K'_{S0}, $\dot{K}_{S0}$ and γ_0 are considered, depending on the values of K'_{T0} and q. K_{S0} and G_0 of magnesio-wüstite are corrected for the volumetric fraction of iron for, but no correction is applied for perovskite.

[f] [28].

[g] [25].

[h] [26].

[i] [27].

temperature and uncertainty. At a given depth, we estimated a probability density function $f(T)$ defined by:

$$f(T)=\int_{\Omega} c(T,\omega)d\Omega, \quad \begin{cases} c(T,\omega) = 1-|x(T,\omega)| & |x(T,\omega)|\le 1 \\ c(T,\omega) = 0 & |x(T,\omega)|>1 \end{cases} \tag{10}$$

where Ω is the model space, i.e., the set of all the possible combinations ω of the thermoelastic parameters and composition, $x(T,\omega)$ is the relative difference (in percent) between PREM and the predicted velocities and density. The closer the prediction to PREM, the more weight it carries. The first order moment of $f(T)$ defines the average temperature, which is a measure of the temperature that gives the best fit to PREM, and the second-order moment defines the standard deviation, which indicates the range of temperatures that fit PREM within the given error bar. Average potential temperatures are more useful for comparison with dynamic models, whereas average mantle temperatures are more easily understood. We also calculated average and standard deviation for compositional parameters (volumetric fractions of perovskite, iron, and calcium).

3. Parameterizing the mantle density and elastic properties

Ab initio calculations started to provide values of density and elastic moduli directly at mantle temperature and pressure [13,32]. They offer the advantage of eliminating uncertainties due to EOS modelling. However, ab initio calculations are extremely time-consuming, and data points are still scarce. We propose here to combine EOS modelling and existing high temperature and pressure data points from ab initio calculations. This reduces potential errors due to EOS and allows the flexibility of a finer depth

parameterization of mantle properties. In our formulation, a thermodynamic parameterization consists of high-pressure and high-temperature extrapolations, and of a set of parameters at ambient temperature and pressure. The consistency of a given parameterization can then be compared to ab initio calculations. In all the calculations of this section, we considered pure Mg-perovskite, thus no iron correction.

We have tested BM3 against recent ab initio calculations at high temperature and pressure [23,32]. First, we used the thermoelastic parameters at ambient pressure and temperature given by ab initio calculations at zero pressure [23] (second column in Table 1). For bulk modulus, we found a very good agreement between the high-temperature extrapolation at ambient pressure (bottom curve in Fig. 1) and the ab initio calculations at zero pressure [23], which justify the use of Eqs. (1) and (2) for perovskite. High-temperature extrapolations for density are

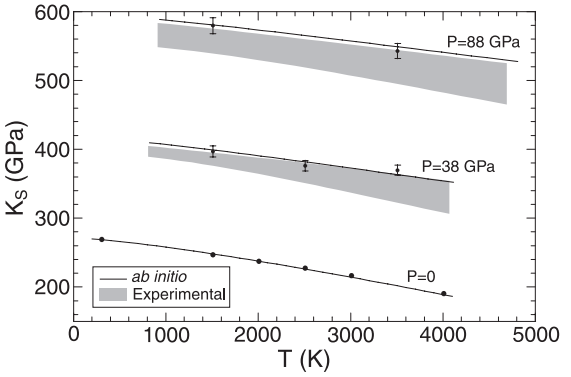

Fig. 1. Extrapolation of the bulk modulus of $MgSiO_3$ perovskite at high temperature and high pressure. Results are presented as a function of the final temperature. The bulk modulus of $MgSiO_3$ perovskite is extrapolated to high temperature and several values of the pressure ($P=0$, $P=38$ GPa and $P=88$ GPa). At $P=0$, the black dots represent ab initio calculations at zero pressure [23], and the plain curve is obtained from high-temperature extrapolation (Eq. (2)). Black dots are obtained by converting K_T values of [23] into K_S values, using the thermal expansion and Grüneisen parameter of [23]. At $P=38$ GPa and $P=88$ GPa, the black dots with error bars represent ab initio calculations at high pressures and temperatures [32], and the curves result from extrapolations at high temperature and BM3 adiabatic compressions. The thermoelastic properties of perovskite are after Oganov et al. [23], and are listed in Table 1, second column. For comparison, the grey shaded areas represent the ranges of values predicted by experimental data (Table 1, first column).

in equally good agreement with [23]. The high-pressure extrapolations for the bulk modulus (Fig. 1, middle and top curves) are in good agreement with the ab initio values of K_S reported in [32]. To estimate K_{S0} and K'_{S0}, Oganov et al. [23] fitted the Vinet EOS [33] to their athermal data, the thermal contribution being obtained with the Mie–Grüneisen–Debye description. Our results thus reconfirm that an adiabatic BM3 compression is consistent with the Mie–Grüneisen–Debye description of thermal pressure together with an isothermal part, as previously shown in [11]. We can now check the consistency between experimental and ab initio data, by using experimental data at ambient pressure and temperature (Table 1, first column) in BM3. Within error bars, there is a reasonable agreement (overlapping ranges) between these high-pressure, high-temperature extrapolations (Fig. 1, shaded areas), and the ab initio calculations (black dots with error bars). Ab initio data are close to the upper bound predicted by experimental data at both $P=38$ GPa and $P=88$ GPa, mainly because K'_{S0} for ab initio data is higher. It is interesting to note that there appears no need for a cross-derivative $\partial^2 K_S/\partial T \partial P$ to predict the bulk modulus correctly (slopes in Fig. 1 are in good agreement). For density, no error bars are given for the ab initio calculations, but the agreement is very good (within 1.0%). Finally, the effective thermal expansion calculated from the temperature derivative of density falls within the error bars in [32].

More serious problems arise when modelling the shear modulus at high pressures and temperatures. Very few experimental data exist for its derivatives. We have investigated the influence of the experimental values of the elastic moduli derivatives on the average potential temperature (Fig. 2). The most sensitive parameter is the pressure derivative, $(G'_0)_{pv}$ (Fig. 2a). The average temperature is about 1800 K if $(G'_0)_{pv}=1.4$, and 3400 K if $(G'_0)_{pv}=2.2$. If $(G'_0)_{pv}\geq 2.0$, very few models fit PREM within 1%, suggesting that high values of $(G'_0)_{pv}$ are unlikely. We then computed the shear modulus at $T_p=298$ K as a function of pressure using values of $(G'_0)_{pv}$ between 1.4 and 2.2. We compared the results with ab initio data in [23], and found that $(G'_0)_{pv}=1.5\pm0.05$ predicts ab initio data best. Note that this value of $(G'_0)_{pv}$ is close to the experimental lower bound in [34]. The temperature derivative $(\dot{G}_0)_{pv}$ is very poorly

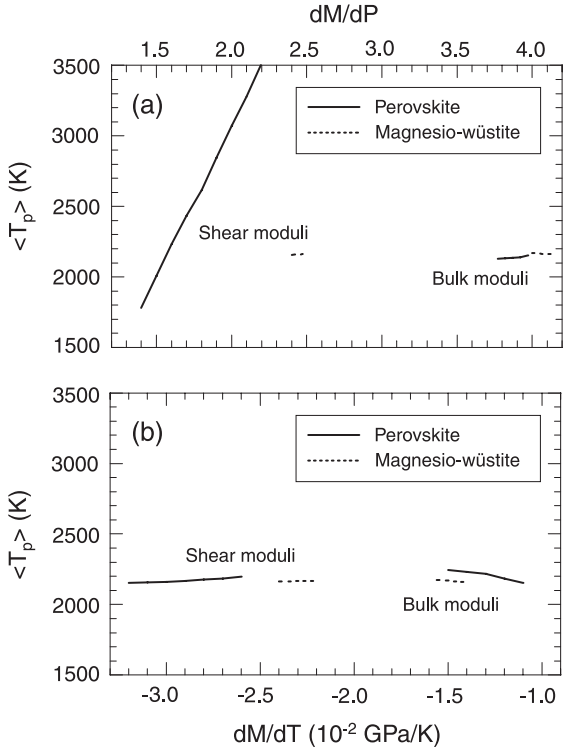

Fig. 2. Sensitivity of the average potential temperature $<T_p>$ to the derivatives of elastic moduli of perovskite (plain curves) and magnesio-wüstite (dashed curves). (a) Pressure derivatives; (b) temperature derivatives. Elastic derivatives are varied within their experimental range (Table 1), and the volumetric fraction of perovskite is equal to 0.8. The average potential temperature is estimated from a collection of models that fit PREM within 1%. Calculation are made at $P=88$ GPa ($z\sim 2000$ km).

constrained. Experimental data [34] give $(\dot{G}_0)_{pv}=-0.029\pm0.003$ GPa/K. Jackson [11], however, proposed a value around -0.020 GPa/K, and ab initio calculations [13] suggest an even lower value of -0.012 GPa/K. We have tested several values of $(\dot{G}_0)_{pv}$ between -0.032 and -0.012 GPa/K, but none of them could explain the ab initio calculations [32] simultaneously at $P=38$ GPa and $P=88$ GPa. At $P=38$ GPa, ab initio data are close to the upper bound predicted by experimental data, whereas at $P=88$ GPa they are close to the lower experimental bound (shaded areas in Fig. 3), but neither the data of Oganov et al. [32] nor those of Marton and Cohen [13] are correctly predicted as a function of temperature. A possible source for this disagreement could be Eq. (3). We repeated calculations using a projection similar to Eq. (2) (with $\delta_S=-1/(\alpha G)\dot{G}_0$), but the disagreement remained. This suggests that a cross-derivative $\partial^2G/\partial T\partial P$ is needed at zero pressure to predict the ab initio shear modulus. We did a systematic search for $\partial^2G/\partial T\partial P$, and found the best agreement with [32] for the empirical relation:

$$\partial^2G/\partial T\partial P=a(\dot{G}_0)_{pv}+b \tag{11}$$

where $a=-1.2\times10^{-2}$ GPa^{-1} and $b=-3.3\times10^{-4}$ K^{-1}. Taking $(\dot{G}_0)_{pv}=-0.020\pm0.008$ and the previous parameterization for the cross-derivative, our EOS modelling of $(G_0)_{pv}$ explain ab initio calculations in [13,32] well indeed (Fig. 3). It is worth noting, from results at $P=38$ GPa, that ab initio calculations favors low values of $(\dot{G}_0)_{pv}$ (-0.012 to -0.020 GPa/K) compared to the published experimental value (-0.029 ± 0.003 GPa/K).

Comparing this modified BM3 to predict ab initio values of G with that obtained from experimental data alone, it appears, unless $(G'_0)_{pv}$ is on the low end of the experimental data and that our ad hoc cross-

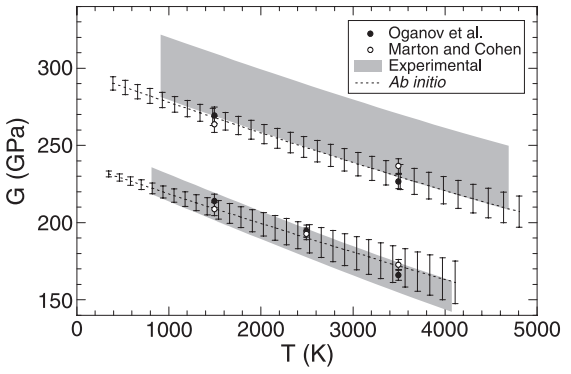

Fig. 3. Extrapolation of the shear modulus of $MgSiO_3$ perovskite at high temperature and high pressure. Results are presented as a function of the final temperature, and two values of the pressure ($P=38$ GPa and $P=88$ GPa). The black and the white dots represent the ab initio calculations at high pressure [32] and temperature [13], respectively. The dashed curves show the average values of the shear modulus predicted by an extrapolation at high temperature and an adiabatic Birch–Murnaghan compression to the third order, in which a cross-derivative is prescribed $\partial^2G/\partial T\partial P$ (see text), and the error bars cover one standard deviation around the average. The pressure and temperature derivative are $(G'_0)_{pv}=1.5\pm0.05$ and $\dot{G}_0=-0.020\pm0.008$ GPa/K, respectively. The shaded areas represent the ranges of values predicted by experimental data (Table 1, first column).

derivative is confirmed by further experimental data, that there is some disagreement between ab initio and experimental data.

4. Average temperature and composition

To estimate the average potential temperature and composition and their standard deviations, we tested a whole collection of models against density and the elastic moduli of PREM. Different criteria can easily lead to different results though. Effects of anelasticity and the uncertainty on the volumetric fraction of iron persuaded da Silva et al. [12] not to use density and the shear modulus. Anelasticity could have minor consequences (see below), but uncertainty in the volumetric fraction of iron can easily be accounted for by varying it within a reasonable range. Using bulk modulus or density alone however does not give tight constraints on the temperature. With the bulk modulus, we find standard deviations of about 600 K for temperature, regardless of depth. Using simultaneously the bulk modulus and density, the standard deviation reduces to 500 K. Composition is better constrained than temperature, but standard deviations are still high (about 12% and 4.5% for perovskite and iron, respectively).

Because very little can be said if average temperature and composition are obtained from the bulk modulus and/or density alone, we decided to use the shear modulus together with the bulk modulus and the density to estimate the average temperature and composition. We varied T_p between and 1500 and 5000 K, X_{pv} between 50% and 100%, Fe_{glob} between 5% and 20%, X_{Ca} between 0% and 12%, and K_{Fe} between 0.2 and 0.5. We did calculations from $z = 800$ km down to the CMB, and omitted the lower mantle top layer ($660 \leq z \leq 800$ km). The reason is that the transformation of garnets into perovskite is probably not fully completed at these depths. Our model accounts for perovskite and magnesio-wüstite only, and may therefore not apply here. We performed three different calculations to emphasize the most important variables. The first one uses ab initio data (second column in Table 1) together with $(G_0')_{pv} = 1.5 \pm 0.05$, $(\dot{G}_0)_{pv} = -0.020 \pm 0.008$ GPa/K, and the empirical relation (11), as explained above. Elastic moduli are corrected for the volumetric fraction of iron following [11]. More recent studies for perovskite [24] and magnesio-wüstite [28] suggest that iron corrections are more significant (Table 1), and they may strongly influence the inferred average temperatures and composition [35]. The second calculation also uses the ab initio data, and accounts for the latest iron corrections [24,28]. Finally, the third calculation uses the experimental data for Mg-perovskite (first column in Table 1), and the full iron corrections. For each calculation, average temperature and composition are computed from models that fit PREM within 1%.

4.1. Statistical profiles obtained with ab initio data

4.1.1. Iron correction from [11]

The plain curves in Fig. 4 represent the mean values of T_p, X_{pv}, and Fe_{glob} obtained with ab initio data and the iron correction from [11]. The shaded grey areas cover one standard deviation around these mean values.

4.1.1.1. Potential temperature (Fig. 4a, grey shaded area). Down to $z = 1600$ km, the average potential temperature is nearly constant around 2050 K. It increases slightly ($dT/dz = 0.14$ K/km) between $z = 1600$ km and $z = 2500$ km, and very rapidly ($dT/dz = 1.8$ K/km) in the lowermost mantle ($2750 \leq z \leq 2880$ km), reaching 2410 K at the CMB. Uncertainties vary between 90 and 260 K, depending on depth. They reach 260 K at the bottom of the mantle. The smallest uncertainties are found around $z = 1600$ km. Within error bars, a purely adiabatic temperature profile could just about be accepted. A possible candidate for superadiabaticity is the lowermost layer, which extends from $z = 2750$ km down to the CMB. In this layer, the mean temperature increases strongly due to gradients in PREM. Error bars are such that robust estimates of the thickness of this layer are difficult.

Fig. 5 compares our temperature estimates together with previously published geotherms. For convenience, results are shown as final temperatures instead of potential temperatures. da Silva et al. [12] reported a strong departure from adiabaticity from $z = 1600$ km down to the CMB (black dots with error bars). Our results rule out such temperature gradients, and predict a cold lowermost mantle compared to [12]. The difference reaches about 1000 K at the CMB. A

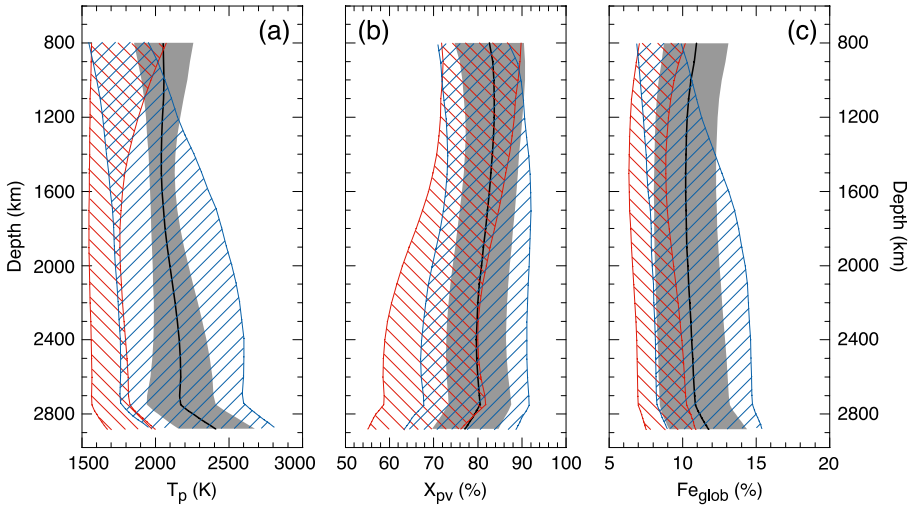

Fig. 4. Statistical profiles of potential temperature (a), volumetric fraction of perovskite (b), and volumetric fraction of iron (c). Plain curves represent the mean profiles obtained when temperature and pressure derivatives of the shear modulus of perovskite are modeled using ab initio data, with iron correction from [11]. The shaded areas cover one standard deviation around these mean profiles. The red dashed areas are obtained using the same modelling, but the correction of elastic moduli for the iron content are taken from [24,28]. The blue dashed areas represent the profiles obtained from experimental data. T_p is varied between 1500 and 5000 K, X_{pv} between 50% and 100%, and Fe_{glob} between 5% and 20%.

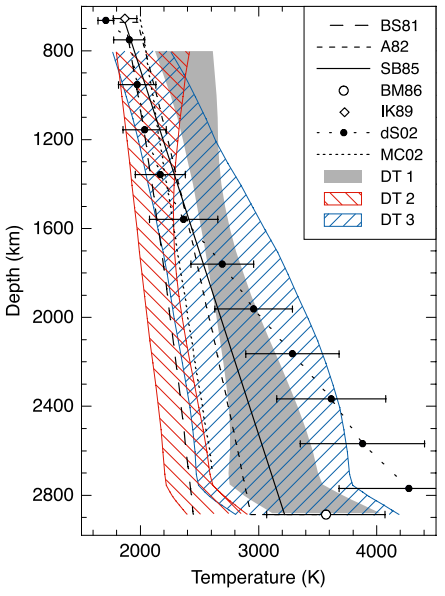

Fig. 5. Comparison between final temperature estimates (DT 1 to 3) from Fig. 4 and previous studies. The colour code is the same as in Fig. 4. BS81, Brown and Shankland [6]; A82, Anderson [4]; SB85, average profile of Shankland and Brown [9]; BM86, Brown and McQueen [3]; IK89, Ito and Katsura [1]; dS02, da Silva et al. [12]; MC02, Marton and Cohen [13].

possible reason for this difference is that da Silva et al. [12] allow much higher values for the Grüneisen parameter at ambient temperature and pressure, and that they test temperature against the bulk modulus only. The long dashed curve represents a profile of temperature reconstructed from the entropy and average seismic profiles [6]. This profile is nearly adiabatic, and because it anchors at $T=1873$ K at $z=670$ km, it is colder than our temperature estimates whatever the depth (see below). The profile calculated in [4] is also slightly colder than our lower estimates, except in the bottom layer ($z=2400$ km down to the CMB), where the agreement is good. The range of temperature proposed in [9] is globally in good agreement with our results, but their gradient is slightly higher. It is worth noting that our estimate of the temperature at the CMB is very close to that predicted in [3] (open dot with error bar), but is difficult to connect with the estimated temperature at the base of the upper mantle [1] (open diamond with error bar).

4.1.1.2. Composition (Figs. 4b–c, grey shaded areas). The mean volumetric fraction of perovskite (X_{pv}, Fig. 4b) is around 83% between 800 and 1600

km, and around 80% between 2000 and 2750 km. In the bottom layer, it decreases more rapidly, and reaches 77% at the CMB. The mean volumetric fraction of iron (Fe_{glob}, Fig. 4c) is close to 10% in most of the lower mantle ($1200 \leq z \leq 2700$ km). At $z = 800$ km and $z = 2800$ km, it is close to 11% and 12%, respectively. Again, steeper variations occur in the lowermost layer. Typically, the standard deviations are close to 6.5–7.5% for perovskite, and 2.0–2.6% for iron.

We also varied the volumetric fraction of Ca-perovskite (X_{Ca}) between 0% and 12% (not shown here). The mean value and standard deviation of X_{Ca} are constant throughout the mantle, and equal to $6 \pm 4\%$. The presence of Ca-perovskite is therefore only weakly constrained. The reason is that density and seismic velocities are not very sensitive to Ca-perovskite. Following [15], we computed sensitivities of density and seismic velocities to calcium, and found that they are one order of magnitude smaller than those for iron. The lack of resolution for X_{Ca} does not significantly change the determination of the mantle average temperature and other compositional parameters. Indeed, the mean temperature calculated with $X_{Ca} = 10\%$ is only 40 K higher than that for $X_{Ca} = 0$. Most of this difference is due to the high value of the pressure derivative of the shear modulus of Ca-perovskite reported in [30]. If, as expected, Ca-perovskite enters the composition of the lower mantle for 6–12% in volume (e.g., [2]), the effects on density and the elastic moduli would be of second-order compared to other compositional parameters. Aluminium perovskite, for which very few data are available, could have more dramatic effects (see Discussion below).

The mantle average composition derived from our calculations strongly supports the pyrolitic model ($X_{pv} = 84\%$ and $Fe_{glob} = 12\%$). Within our error bars, we do not see strong evidence for or against chemical stratification. The average composition proposed by Jackson [11] is significantly poorer in perovskite ($X_{pv} = 67\%$), but assumes an adiabatic profile with $T_p = 1600$ K. This discrepancy can be fully explained by the trade-offs existing between temperature and composition (Section 5 and Fig. 7). Marton and Cohen [13] recently proposed an even smaller value of $X_{pv} = 54\%$. Since they use a relatively cold adiabat ($T_p = 1800$ K, short dashed curve in Fig. 5), part of the discrepancy can be accounted for by the trade-offs between temperature and composition. Additional differences probably result from their low value of the iron partitioning ($K_{Fe} = 0.1$).

4.1.2. Full iron corrections

The red dashed areas in Fig. 4 cover one standard deviation around the average profiles obtained with the iron corrections from [24,28]. As expected, results are significantly different from those obtained with the iron correction from [11]. Temperatures are colder by 200 K at $z = 800$ km, and 600 K at $z = 2800$ km. The Average temperature strongly increases between 2750 and 2880 km ($dT/dz = 1.1$ K/km), but within error bars a purely adiabatic profile is possible. Additional calculations (not shown here) show that most of the difference is due to the correction for the elastic moduli of magnesio-wüstite [28]. Temperature profiles that account for the correction for the elastic moduli of perovskite [24] only are colder by 100 K at most. Inferred final temperatures (red dashed area in Fig. 5) connect well with the temperature estimates at the base of the upper mantle [1], and agree with adiabatic profiles such as in [6]. The upper bound is close to the profile derived in [13], but at the CMB it fails to connect with the range of the anchoring point [3].

Inferred composition also changes significantly, although less dramatically than temperature. Overall, the composition derived with full iron correction is less rich in perovskite and iron. On average, X_{pv} is close to 80% down to $z = 1500$ km and decreases to 65% at $z = 2800$ km, although a perovskite fraction of 75% is possible within error bars. The mean value of Fe_{glob} remains between 7.5% and 9.0% throughout the lower mantle. It is interesting to note that Fe_{glob} is better constrained (standard deviation is between 1.3 and 1.7) when corrections [24] and [28] are used.

4.2. Statistical profiles obtained with experimental data

The profiles for experimental data are represented by blue dashed areas in Fig. 4. Compared to the ab initio results, the mean potential temperature increases more rapidly with depth, and the standard deviations are higher, around 320 K. Within error bars, a purely adiabatic temperature profile is just about possible. At

$z = 800$ km, the average temperature is $T_p = 1900$ K, and it connects well with the estimated temperature at $z = 660$ km. At the CMB, the value of T_p is higher by 200 K than that obtained with ab initio data, and falls in the upper bound proposed by [3]. The mean volumetric fractions of perovskite and iron slightly increase with depth (from 81% to 86% for perovskite, and from 10% to 13% for iron), with higher standard deviations (up to 8.5% for perovskite and 3.3% for iron). In general, experimental data alone give higher uncertainties in temperature, perovskite and iron profiles, and are not very sensitive to the applied iron correction in the individual minerals.

4.3. Consequences for mantle dynamics

Our results suggest that a large collection of combinations T_p, Fe_{glob}, and X_{pv}, given the ranges of thermoelastic parameters, fit PREM as defined in Eq. (10). An accurate modelling of the shear modulus allows a significant reduction of the error bars, but the standard deviations are still high, around 300 K for temperature, 8.0% for perovskite, and 3.0% for iron. Some trade-offs exist between the parameters (in particular between temperature and composition), which is the reason why such a wide range of models fit PREM (see Discussion below). When ab initio data are used, the inferred temperatures are very sensitive to the applied correction for the iron content.

The temperature profiles plotted in Fig. 4a have different implications for mantle dynamics. Ab initio data for the elastic moduli of perovskite together with an iron correction from [11] predict a hot lower mantle. The inferred temperature at the top of the lower mantle ($z = 800$ km) does not connect to the estimates at $z = 660$ km [1,2], implying that the mantle is not adiabatic in this layer. Chemical transformations may participate to this non-adiabaticity, but a thermal boundary layer is certainly also present. Another thermal boundary layer is likely to be present somewhere in the mid- or lowermost mantle. Ab initio data together with recent iron corrections [24,28] predict a cold mantle. The inferred temperature connects to the estimates at $z = 660$ km [1,2], but not those at the CMB [3], implying the presence of a thin thermal boundary layer at the bottom of the mantle. When experimental data are used, the temperature profile connects the estimated temperatures at both $z = 660$ km and the CMB, and there is no need for a thermal boundary layer around this depth. On the other hand, the temperature gradient is such that at least one thermal boundary layer must be present somewhere between the mid–lower mantle and the CMB. Finally, all data sets predict error bars on composition that

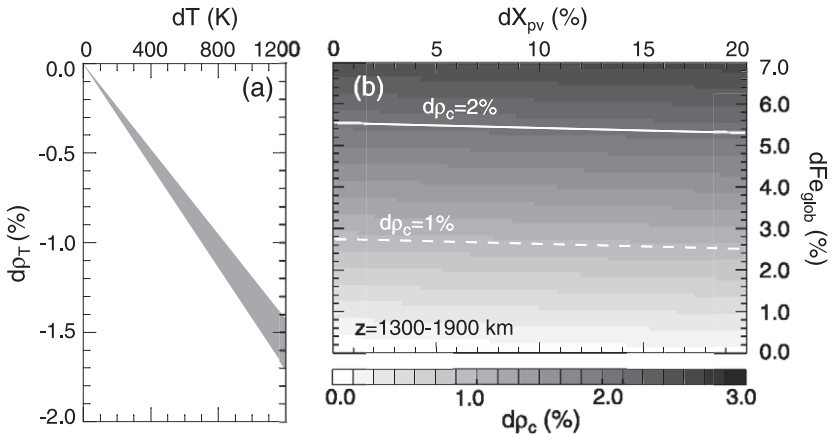

Fig. 6. Radial density variations in the mid-mantle ($1300 \le z \le 1900$ km). (a) Density variations due to temperature variations. The shaded area covers one standard deviation around the mean value of $d\rho_T$. (b) Density variations due to chemical changes (perovskite and iron). Standard deviations in $d\rho_c$ are close to 20% of the plotted values. The white dashed and plain lines denote $d\rho_c = 1\%$ and $d\rho_c = 2\%$, respectively. Sensitivity of density to temperature, perovskite, and iron are averaged between $z = 1300$ km and $z = 1900$ km. The correction of elastic moduli for iron content is taken from [24,28].

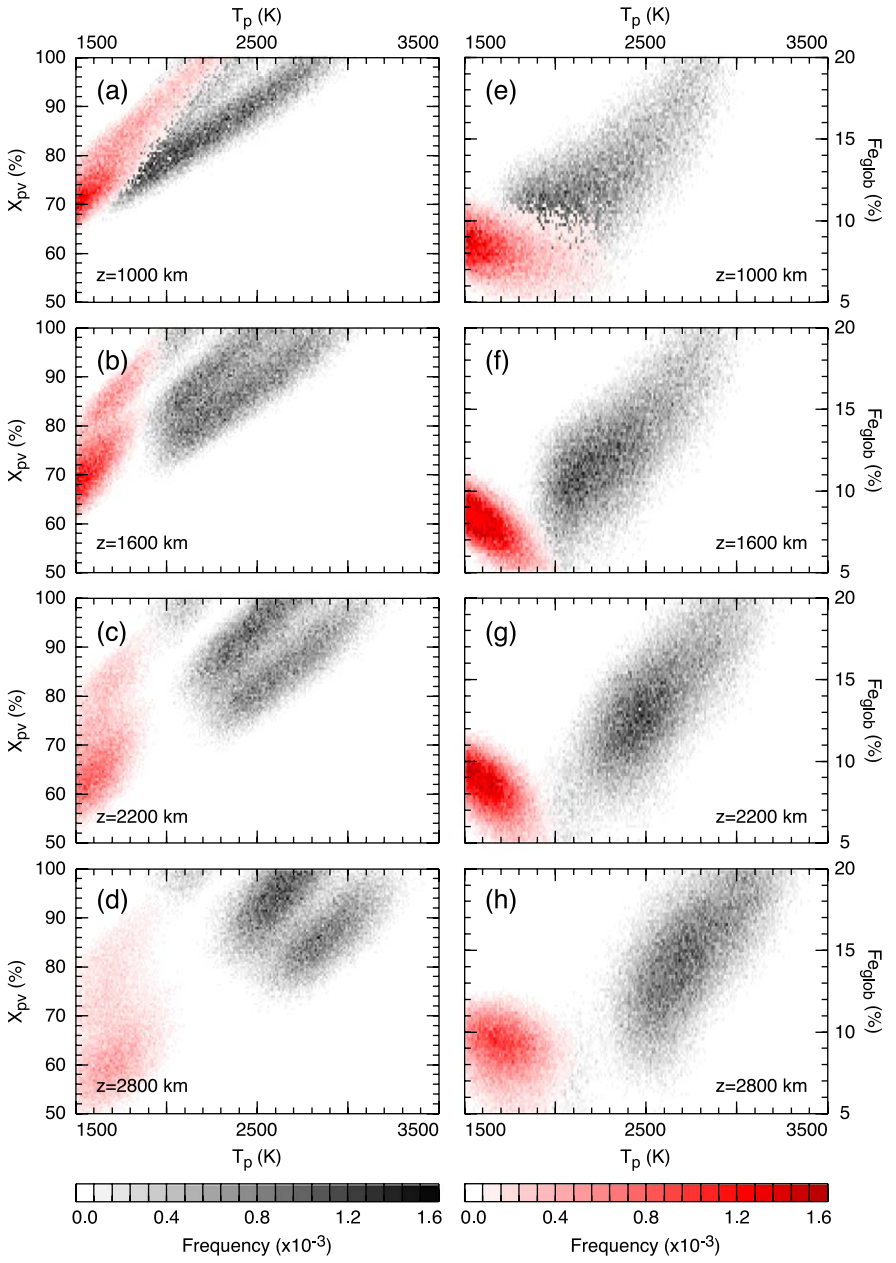

Fig. 7. (a–d) Frequency as a function of potential temperature (T_p), and volumetric fraction of perovskite (X_{pv}). (e–h) Frequency as a function of potential temperature (T_p), and global volumetric fraction of iron (Fe_{glob}). Two series of calculations are represented. One using iron correction from [11] (grey color scale), and one using full iron correction, including [24,28] (red color scale).

allow significant chemical variations (perovskite and/or iron).

It is interesting to test the hypothesis of a strongly stratified mantle against the profiles of temperature and composition shown in Fig. 4. We reconstructed variations of density from maximum allowed variations of temperature and composition, and from appropriate sensitivities of density to temperature and

composition. Using the approach of Trampert et al. [15], we have computed the sensitivities of density to temperature, perovskite and iron as a function of depth. Note that sensitivities of density (shear velocity) to perovskite and iron depend somewhat (strongly) on the applied correction for the iron content. Uncertainties in these sensitivities are used to estimate uncertainties on density.

To investigate the possible presence of a distinct mid-mantle layer, we averaged the sensitivities of density between $z=1300$ km and $z=1900$ km, and estimated density variations induced by purely thermal and compositional variations (Fig. 6). For instance, a temperature variation of 800 K across this layer would result in a thermal density contrast $d\rho_T=(-1.04\pm0.09\%)$ (Fig. 6a). From ab initio data, we see that the average temperature cannot not increase by more than 200 K between $z=1300$ km and $z=1900$ km, and therefore $d\rho_T=(-0.26\pm0.03\%)$ is an upper limit for the thermal density contrast. If experimental data are used, larger variations are possible (up to 800 K), and the maximum value of $d\rho_T$ is equal to $(-1.04\pm0.09\%)$. Density contrasts due to pure chemical variations ($d\rho_c$) are plotted in Fig. 6b. Variations in perovskite alone give small density contrasts, up to $d\rho_c=0.11\%$ for a 20% excess in perovskite. As expected, iron has stronger effects. For an excess in iron of 3% (5%), the density contrast is equal to 1.1% (1.8%). Davaille [21] showed that the doming regime should occur for a chemical density contrast around 1%. Variations in perovskite alone cannot produce such a contrast. One needs an additional 2.5–3% enrichment in iron, depending on the excess in perovskite (white dashed line in Fig. 6b). A strongly stratified convection requires a chemical density contrast higher than 2%. Assuming a maximum excess in perovskite of 20%, this value can only be reached for excess in iron higher than 5.2% (white plain line in Fig. 6b). Given the maximum ranges allowed by ab initio data between $z=1300$ km and $z=1900$ km (see red dashed areas in Fig. 4b–c), a chemical density contrast higher than 2% can hardly be obtained. The results above have been obtained for full iron corrections, including [24,28]. If only corrections from [11] are used, the values change slightly, but the conclusions remain the valid. Experimental data allow larger variations (up to 7% for iron), and therefore higher chemical density contrasts. We repeated these calculations for a distinct layer close to the CMB, and found similar results. Although the sensitivity of density to perovskite is higher, one still needs at least 5.0% enrichment in iron to create a 2% chemical density contrast.

Models of strongly stratified convection [18–22], which require average variations of thermal density bigger than 0.3% and average variations of chemical density larger than 2%, are not consistent with the average temperature and composition predicted by ab initio data. If by contrast, the average composition is inferred from experimental data, more uncertainty is obtained, and a strong stratification cannot be completely excluded ($d\rho_T$ is up to -1.0%, and $d\rho_c$ is up to 2.6%). Note that this analysis is based on average temperature and composition jumps. If lateral variations of temperature and composition are present, these conclusions can change locally.

5. Discussion

Average seismic models provide most information on the average Earth, but do not fully constrain the average mantle temperature and composition. The reason is that errors in the sensitivities of seismic velocities and density, and uncertainties in thermoelastic parameters are such that temperature and composition cannot be unambiguously determined. To quantify the trade-off between two given parameters x and y, we have calculated the frequency as a function of x and y in a similar way to the frequency for temperature (Eq. (10)). Fig. 7 shows the frequency as a function of potential temperature and volumetric fraction of perovskite (a–d) or volumic fraction of iron (e–h). The applied correction for iron is either taken from [11] (black dots), or from [24,28] (red dots). A trade-off indicates that high and low values of T_p explain PREM equally well, if they are associated with high and low values of X_{pv}, respectively. This trade-off has already been reported [11,13,16,17], and is particularly strong at the top of the lower mantle (Fig. 7a). It gets slightly smaller in the deeper mantle (Fig. 7d), but is present independently of the applied correction for iron content. Jeanloz and Knittle [10] pointed out a trade-off between the temperature and the volumetric fraction of iron. When the applied correction for iron is from [11], we also observe this

trade-off at every depth (Fig. 7e–h). Simultaneous low temperature and low volumetric fraction of iron explain as well PREM as simultaneous high temperature and high volumetric fraction of iron. When we use the corrections given in [24,28], we do not see any significant trade-off.

So far, we have only considered the effects of variations in the global volumetric fraction of iron and calcium. Aluminium oxide (Al_2O_3) may be also present for 4–5 mol%. At mantle temperature and pressure, it is thought to be incorporated into (Mg,Fe)-perovskite. The few laboratory measurements available for these phases (e.g., [36,37]) suggest that their elastic properties are significantly different from those of (Mg,Fe)-perovskite. These experimental results contrast strongly with ab initio calculations for elastic properties of aluminium oxide (Al_2O_3), which are close to those for Mg-perovskite [38]. Experimental values of the bulk modulus have important consequences on the determination of the potential temperature. If Al-perovskite is present for 4% in volume, the temperature is lower by 150–200 K, depending on the depth. However, the number of models that fit PREM within 1% decreases strongly with increasing volumetric fraction of aluminium (X_{Al}). Effects induced by variations in the derivatives of the bulk modulus are particularly dramatic. For $X_{Al}=2\%$, only a small amount of models fit PREM within 1%, and the mean potential temperature is smaller than that for $X_{Al}=0$ by more than 1000 K. For values of X_{Al} higher than 3%, we do not find any model that fit PREM within 1%. Given the experimental values to date, the presence of 4–5 mol% of Al-perovskite in the lower mantle is unlikely. The available ab initio values indicate that the presence of Al-perovskite could have a limited influence on the determination of the mantle temperature. Aluminium probably plays an important role, but additional experiments and/or ab initio calculations need to be conducted for a better knowledge of the elastic parameters of Al-perovskite.

Mineral physics measurements are made at much higher frequencies than seismic observations, If attenuation is present, this could possibly affect the comparison. It has been argued that this is important for the temperature sensitivity of seismic wave speed [39,40], but using most recent data, Trampert et al. [15] showed that this effect is modest in the lower mantle. These results cannot be used in a straightforward manner because here we are comparing calculations of absolute wave speeds to PREM. Seismic attenuation can significantly vary speed (up to 1%). This means that totally different combinations of temperature and composition will be selected to fit PREM. We introduced attenuation using the relation for dissipation of phase speed proposed by Minster and Anderson [41], and found that the estimated temperature curve would shift towards lower values by 100 K at most. Composition would also shift according to the trade-offs. This is clearly insignificant given overall errors. It is however not obvious that seismic attenuation is the right way to extrapolate dispersion from experimental studies to seismic conditions [42,43]. A recent review of measurements [43] showed complicated effects of frequency, temperature and grain size. Data are still lacking to make firm statements on the lower mantle, but it could possibly affect inferences.

6. Conclusions

The average temperature and composition of the lower mantle are key parameters for testing different possible models of mantle dynamics. We tested high pressure and temperature data from ab initio calculations and mineral physics experiments against PREM to constrain the mantle temperature and composition. We showed that, although it is least well known, the shear modulus significantly reduces uncertainty on temperature and composition, but experimental and ab initio data appear to be inconsistent. Using the ab initio data, inferred temperatures are very sensitive to the applied correction for the iron content. The temperature predicted by experimental data alone has a steeper gradient and larger uncertainties than that obtained with ab initio data, regardless of the iron correction. A strong chemical stratification ($d\rho_c \geq 2\%$) in the mid-mantle is unlikely within the error bars from ab initio data, but possible with experimental data. Other sources of uncertainty are the trade-offs between temperature and composition. An interesting remaining question concerns the presence of Al-perovskite in the mantle. If the present available measurements are correct, only very low values of temperature are able to fit PREM. Measured frequency effects in the laboratory are different from frequen-

cy effects predicted by seismic attenuation models. This could influence results, and needs to be quantified in future work.

Acknowledgements

We are grateful to Dave Yuen and Ian Jackson for useful and constructive comments on a first version of this paper. We thank Mark Bukowinski and an anonymous reviewer for their helpful reviews, and Scott King for constructive comments. This research was funded by Utrecht University. ***[SK]***

References

[1] E. Ito, T. Katsura, A temperature profile of the mantle transition zone, Geophys. Res. Lett. 16 (1989) 425–428.
[2] J. Ita, L. Stixrude, Petrology, elasticity and composition of the mantle transition zone, J. Geophys. Res. 97 (1992) 6849–6866.
[3] J.M. Brown, R.G. McQueen, Phase transitions, Grüneisen parameter, and elasticity for shocked iron between 77 and 400 GPa, J. Geophys. Res. 91 (1986) 7485–7494.
[4] O.L. Anderson, The Earth's core and the phase diagram of iron, Philos. Trans. R. Soc. Lond., A 306 (1982) 21–35.
[5] A.M. Dziewonski, D.L. Anderson, Preliminary reference Earth model, Phys. Earth Planet. Inter. 25 (1981) 297–356.
[6] J.M. Brown, T.J. Shankland, Thermodynamic parameters in the Earth as determined from seismic profiles, Geophys. J. R. Astron. Soc. 66 (1981) 579–596.
[7] G.F. Davies, A.M. Dziewonski, Homogeneity and constitution of the Earth's lower mantle and outer core, Phys. Earth Planet. Inter. 10 (1975) 336–343.
[8] T.S. Duffy, D.L. Anderson, Seismic wave speeds in mantle minerals and the mineralogy of the upper mantle, J. Geophys. Res. 94 (1989) 1895–1912.
[9] T.J. Shankland, J.M. Brown, Homogeneity and temperatures in the lower mantle, Phys. Earth Planet. Inter. 38 (1985) 51–58.
[10] R. Jeanloz, E. Knittle, Density and composition of the lower mantle, Philos. Trans. R. Soc. Lond., A 328 (1989) 377–389.
[11] I. Jackson, Elasticity, composition and temperature of the Earth's lower mantle: a reappraisal, Geophys. J. Int. 134 (1998) 291–311.
[12] C.R.S. da Silva, R.M. Wentzcovitch, A. Patel, G.D. Price, S.I. Karato, The composition and geotherm of the lower mantle: constraints from the elasticity of silicate perovskite, Phys. Earth Planet. Inter. 118 (2000) 103–109.
[13] F.C. Marton, R.E. Cohen, Constraints on lower mantle composition from molecular dynamics simulations of $MgSiO_3$ perovskite, Phys. Earth Planet. Inter. 134 (2002) 239–252.
[14] F.D. Stacey, Theory of thermal and elastic properties of the lower mantle and core, Phys. Earth Planet. Inter. 89 (1995) 219–245.
[15] J. Trampert, P. Vacher, N. Vlaar, Sensitivities of seismic velocities to temperature, pressure and composition in the lower mantle, Phys. Earth Planet. Inter. 124 (2001) 255–267.
[16] D.L. Anderson, Theory of the Earth, Blackwell, Oxford, 1989.
[17] L. Stixrude, R.J. Hemley, Y. Fei, H.K. Mao, Thermoelasticity of silicate perovskite and magnesiowüstite and stratification of the Earth's mantle, Science 257 (1992) 1099–1101.
[18] P. Olson, C. Kinkaid, Experiments on the interaction of thermal convection and compositional layering at the base of the mantle, J. Geophys. Res. 96 (1991) 4347–4354.
[19] U.R. Christensen, A. Hofmann, Segregation of subducted oceanic crust in the convecting mantle, J. Geophys. Res. 99 (1994) 19867–19884.
[20] P.J. Tackley, Three-dimensional simulations of mantle convection with a thermo-chemical basal boundary layer: D″? in: M. Gurnis, et al. (Eds.), The Core–Mantle Boundary Region, Geophys. Monogr. Ser., vol. 28, AGU, Washington, DC, 1998, pp. 231–253.
[21] A. Davaille, Simultaneous generation of hotspots and superswells by convection in a heterogeneous planetary mantle, Nature 402 (1999) 756–760.
[22] L.H. Kellogg, B.H. Hager, R.D. van der Hilst, Compositional stratification in the deep mantle, Science 283 (1999) 1881–1884.
[23] A.R. Oganov, J.P. Brodholt, G.D. Price, Ab initio elasticity and thermal equation of state of $MgSiO_3$ perovskite, Earth Planet. Sci. Lett. 184 (2001) 555–560.
[24] B. Kiefer, L. Stixrude, R.M. Wentzcovitch, Elasticity of $(Mg,Fe)SiO_3$-Perovskite at high pressures, Geophys. Res. Lett. 29 (2002) DOI: 10.1029/2002GL014683.
[25] S.V. Sinogeikin, J.D. Bass, Single crystal elasticity of MgO at high-pressure, Phys. Rev., B 59 (1999) 14141–14144.
[26] B.B. Karki, R.M. Wentzcovitch, S. de Gironcoli, S. Baroni, High-pressure lattice dynamics and thermoelasticity of MgO, Phys. Rev., B 61 (2000) 8793–8800.
[27] Y. Sumino, O.L. Anderson, I. Suzuki, Temperature coefficients of elastic constants of single crystal MgO between 80 and 1300 K, Phys. Chem. Miner. 9 (1983) 38–47.
[28] J. Kung, B. Li, D.J. Weidner, J. Zhang, R.C. Liebermann, Elasticity of $(Mg_{0.83},Fe_{0.17})O$ ferropericlase at high pressure: ultrasonic measurements in conjunction with X-radiation techniques, Earth Planet. Sci. Lett. 203 (2002) 557–566.
[29] Y. Wang, D.J. Weidner, F. Guyot, Thermal equation of state of $CaSiO_3$ perovskite, J. Geophys. Res. 101 (1996) 661–672.
[30] B.B. Karki, J. Crain, First-principles determination of elastic properties of $CaSiO_3$ perovskite at lower mantle pressures, Geophys. Res. Lett. 25 (1998) 2741–2744.
[31] B.L.N. Kennett, E.R. Engdahl, R. Bulland, Constraints on seismic velocities in the Earth from travel times, Geophys. J. Int. 122 (1995) 108–124.
[32] A.R. Oganov, J.P. Brodholt, G.D. Price, The elastic constants of MgSiO3 perovskite at pressures and temperatures of the Earth's mantle, Nature 411 (2001) 934–937.
[33] P. Vinet, J. Ferrante, J.H. Rose, J.R. Smith, Compressibility of solids, J. Geophys. Res. 92 (1987) 9319–9325.

[34] Y.D. Sinelnikov, G. Chen, D.R. Neuville, M.T. Vaughan, R.C. Liebermann, Ultrasonic shear wave velocities of $MgSiO_3$ perovskite at 8 GPa and 800 K and lower mantle composition, Science 28 (1998) 677–679.
[35] B.B. Karki, L. Stixrude, Seismic velocities of major silicate and oxide phases of the lower mantle, J. Geophys. Res. 104 (1999) 13025–13033.
[36] J. Zhang, D.J. Weidner, Thermal equation of state of aluminium-enriched silicate perovskite, Science 284 (1999) 782–784.
[37] I. Daniel, H. Cardon, G. Fiquet, F. Guyot, M. Mezouar, Equation of state of Al-bearing perovskite to lower mantle pressure conditions, Geophys. Res. Lett. 28 (2001) 3789–3792.
[38] W. Duan, B.B. Karki, R. Wentzcovitch, High-pressure elasticity of alumina studied by first principles, Am. Mineral. 84 (1999) 1961–1966.
[39] S.-I. Karato, Importance of anelasticity in the interpretation of seismic tomography, Geophys. Res. Lett. 20 (1993) 1623–1626.
[40] S.-I. Karato, B.B. Karki, Origin of lateral variation of seismic wave velocities and density in the deep mantle, J. Geophys. Res. 106 (2001) 21771–21783.
[41] J.B. Minster, D.L. Anderson, A model of dislocation-controlled rheology for the mantle, Philos. Trans. R. Soc. Lond., A. 299 (1981) 319–356.
[42] A. Dewaele, F. Guyot, Thermal parameters of the Earth's lower mantle, Phys. Earth Planet. Inter. 107 (1998) 261–267.
[43] I. Jackson, Laboratory measurement of seismic wave dispersion and attenuation: recent progress, in: S.I. Karato, et al. (Ed.), Earth's Deep Interior: Mineral Physics and Tomography From The Atomic To The Global Scale, Geophys. Monogr. Ser., vol. 117, AGU, Washington, DC, 2001, pp. 63–87.